

# Magnetic ordering and magnetodielectric phenomena in $\text{CoSeO}_4$

Brent C. Melot, Lucy E. Darago, and Ram Seshadri  
*Materials Department and Materials Research Laboratory  
University of California, Santa Barbara CA 93106*

Abby Goldman  
*Physics Department, Mount Holyoke College,  
South Hadley, Massachusetts 01075*

Joshua D. Furman  
*Department of Materials Science and Metallurgy,  
University of Cambridge, U.K. CB2 3QZ*

Efrain E. Rodriguez  
*National Institute of Standards and Technology,  
Gaithersburg, Maryland 20899-6102*

$\text{CoSeO}_4$  has a structure consisting of edge-sharing chains of  $\text{Co}^{2+}$  octahedra which are held together by  $\text{SeO}_4^{2-}$  tetrahedra *via* shared oxygen atoms at the edges of the octahedra. DC magnetization measurements indicate a transition to an ordered state below 30 K. Powder neutron diffraction refinements suggest an ordered state with two unique antiferromagnetic chains within the unit cell. Isothermal magnetization measurements indicate a temperature-dependent field-induced magnetic transition below the ordering temperature. From neutron diffraction, we find this corresponds to a realignment of spins from the canted configuration towards the *c*-axis. The dielectric constant shows a change in slope at the magnetic ordering temperature as well as a quadratic dependence on the external magnetic field.

PACS numbers: 75.50.Ee, 75.30.Kz

## I. INTRODUCTION

Magnetodielectrics are materials in which the dielectric properties couple to changes in the magnetic order. The ability to find and design new single-phase materials which exhibit this coupling between the spin and charge degrees of freedom has significant technological implications in the development of magnetic sensors and field-tunable dielectrics.<sup>1,2</sup> Systems showing incommensurate and noncollinear spin structures such as  $\text{CoCr}_2\text{O}_4$ <sup>3,4</sup>,  $\text{Mn}_3\text{O}_4$ <sup>5</sup>,  $\text{SeCuO}_3$ <sup>6</sup>, and  $\text{Ni}_3\text{V}_2\text{O}_8$ <sup>7</sup> have all been extensively studied to understand the nature of such interactions. Recent work characterizing the magnetoelectric coupling in the magnetic chain compounds  $\text{MnWO}_4$ ,<sup>8</sup> and  $\text{LiCu}_2\text{O}_2$ .<sup>9,10</sup> indicate that systems with reduced crystallographic dimensionality should be of particular interest because of the strong interplay between the charge, lattice, and magnetic degrees of freedom that occurs in these materials.<sup>11,12</sup> Reduced dimensionality has been found to result in noncollinear and canted antiferromagnetic spin structures which break symmetry restrictions and allow electric polarization to develop.

Here we discuss the preparation and detailed magnetic and dielectric characterization of  $\text{CoSeO}_4$ ; a magnetic chain compound which adopts a crystal structure analogous to  $\beta\text{-CoSO}_4$  (Fig. 1). The orthorhombic unit cell contains chains of octahedrally coordinated  $\text{Co}^{2+}$  which are bound together by  $\text{SeO}_4^{2-}$  tetrahedra *via* shared oxygen atoms at the edges of the octahedra. The chains

of octahedra are tilted with respect to neighboring chains with the axis of the octahedra tilted  $-35^\circ$  and  $+35^\circ$  off the *a*-axis for the chains on the edge and in the center of the cell respectively. Previously reports have characterized the nuclear and magnetic structure using neutron diffraction,<sup>13,14</sup> but no reports on the magnetic susceptibility or dielectric properties have been made to date, and the effects of magnetic fields have not been fully investigated. Using detailed magnetization, heat capacity, powder neutron diffraction, and dielectric measurements, we show that the transition to long-range antiferromagnetic below 30 K is accompanied by a significant change in the slope of the temperature dependence of the dielectric constant. We also find a field-induced change in the magnetic structure. The dependence of the dielectric constant on the external field, which is quadratic in nature, changes dramatically above the field-induced magnetic transition.

## II. EXPERIMENTAL METHODS

The title compound was prepared following a previously reported procedure<sup>15</sup> by neutralizing a solution of selenic acid (2.559 g 23.06 mmol) of  $\text{SeO}_2$  dissolved in 50 cm<sup>3</sup> of water) with  $\text{Co}_2\text{CO}_3(\text{OH})_2$  (1.629 g, 7.69 mmol) at 70°C and recrystallizing in water. The final crystallization step was performed by allowing the remaining water to evaporate at room temperature over several

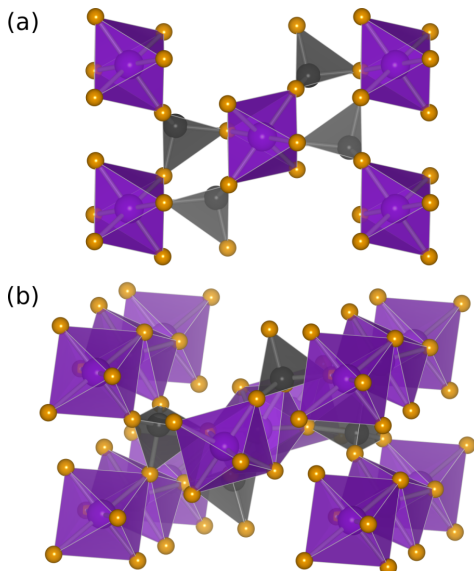


FIG. 1: (Color Online) Illustration of the crystal structure of  $\text{CoSeO}_4$ . Chains of octahedrally coordinated  $\text{Co}^{2+}$  (purple) are bound together by  $\text{SeO}_4$  tetrahedra *via* shared oxygen atoms at the edges of the octahedra. Note that the chains are alternately tilt  $+35^\circ$  and  $-35^\circ$  off the  $a$ -axis. (a) View down the  $c$ -axis of the unit cell. (b) View down the  $c$ -axes to illustrate the chains of edge sharing  $\text{CoO}_6$

days. Faceted crystals of dark red  $\text{CoSeO}_4 \cdot 6\text{H}_2\text{O}$  up to 2 cm on a side were obtained from this procedure. These crystals were ground and dehydrated at  $125^\circ\text{C}$  overnight to yield a bright pink powder of  $\text{CoSeO}_4 \cdot \text{H}_2\text{O}$  which was subsequently heated at  $315^\circ\text{C}$  for several days to produce a light violet powder of anhydrous  $\text{CoSeO}_4$ .  $\text{Co}_2\text{CO}_3(\text{OH})_2$  was prepared following a separate previously reported procedure.<sup>16</sup> Stoichiometric amounts of  $\text{CoNO}_3 \cdot 5\text{H}_2\text{O}$  and  $\text{Na}_2\text{CO}_3$  were separately dissolved in  $\text{H}_2\text{O}$  with a 2:1 ( $\text{NaCO}_3:\text{CoNO}_3$ ) volume excess. The solution of  $\text{CoNO}_3$  was added to the solution of  $\text{Na}_2\text{CO}_3$  which had been preheated to  $90^\circ\text{C}$ . After stirring for 2 hours the resulting dark purple precipitate was collected by vacuum filtration and subsequently washed with  $\text{H}_2\text{O}$  and ethanol. Purity of the precursors and final product was confirmed by powder X-ray diffraction on a Philips XPERT MPD diffractometer operated at 45 kV and 40 mA.

Temperature dependence of the DC magnetization was measured on well-ground powder samples using a Quantum Design MPMS 5XL SQUID magnetometer. The specific heat data were collected using the semiadiabatic technique as implemented in a Quantum Design Physical Property Measurement System (PPMS), under zero applied field as well as under a 50 kOe field. The measurement was made by mixing the compound with equal parts by mass of Ag powder and pressing into a pellet in order to improve thermal coupling to the stage. The contribution from Ag was measured separately and subtracted. Variable temperature neutron diffraction data

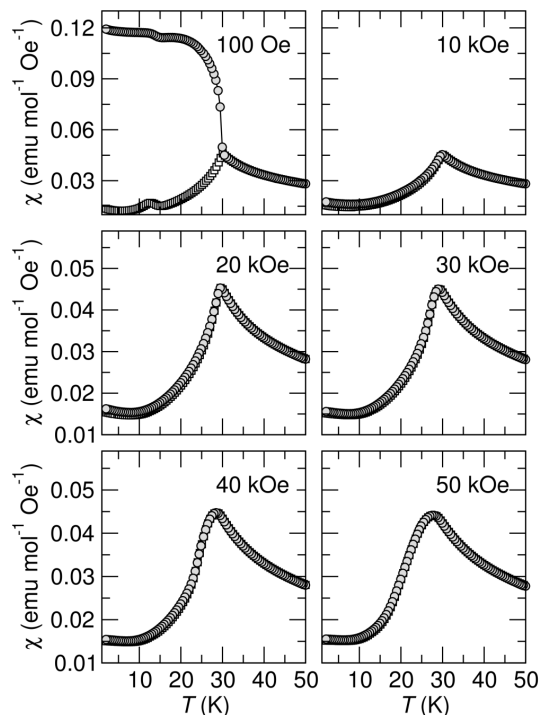


FIG. 2: Field-cooled (FC, open symbols) and zero-field cooled (ZFC, closed symbols) magnetic susceptibility of a powder sample of  $\text{CoSeO}_4$  acquired under increasing strengths of the external magnetic field. At 30 K, the system orders to an antiferromagnetic state. A weak ferromagnetic component is found in the 100 Oe data, suggested from the separating ZFC and FC traces. Note also that the cusp which indicates the magnetic ordering is smeared out with increasing field strength.

under a magnetic field were collected on the BT1 powder diffractometer at the National Institute of Standards and Technology, Gaithersburg, MD using a wavelength of  $2.08 \text{ \AA}$ . Dielectric properties were measured by attaching polished copper electrodes to opposite faces of a cold-pressed pellet of  $\text{CoSeO}_4$ , using a Quantum Design PPMS for temperature and field control, and an Agilent 4980A LCR meter to measure the capacitance.

### III. COMPUTATIONAL METHODS

Density functional theory (DFT) calculations were performed using the Vienna *Ab-initio* Simulation Package (VASP)<sup>17,18</sup> at the experimental lattice parameters. The projector augmented-wave (PAW) method<sup>19</sup> was used together with the local density approximation (LDA) Ceperley-Alder exchange correlation functional.<sup>20</sup> A plane-wave energy cutoff of 500 eV and a  $6 \times 3 \times 9$   $\Gamma$ -centered Monkhorst-Pack<sup>21</sup>  $k$ -point mesh corresponding to 162 irreducible  $k$ -points was used to sample the Brillouin zone. The tetrahedron method with the Blöchl correction<sup>19</sup> was used for Brillouin zone integrations. Correlation was treated using the LDA+U

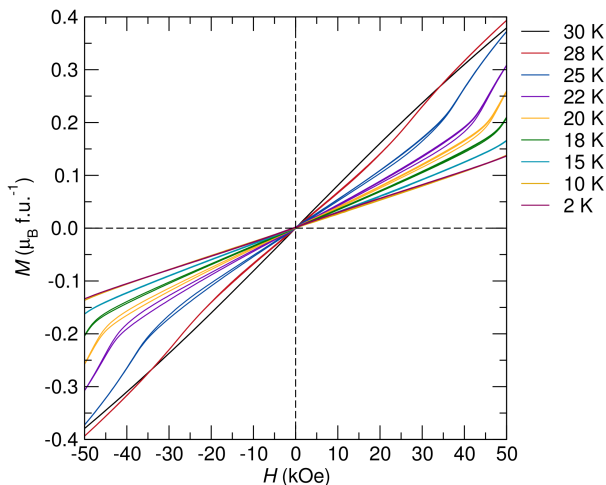


FIG. 3: (Color Online) (a) Isothermal magnetization loops at various temperatures below the Néel temperature. Note the field induced transition which pushes to higher fields at low temperatures.

formalism within the rotationally invariant approach of Liechtenstein *et al.*<sup>22</sup> The applicability of the LDA+ $U$  formalism is validated in the example of  $d^7$   $\text{Co}^{2+}$  because crystal symmetry results in an absence of orbital degeneracy. Several values of  $U$  were tested with only qualitative changes to the band structure being found. Therefore a  $U$  of 5 eV and a  $J$  of 1 eV was chosen to agree with previously published DFT results calculated on octahedrally coordinated  $\text{Co}^{2+}$ .<sup>23</sup>

#### IV. RESULTS AND DISCUSSION

The high temperature region (200 K to 300 K) of the inverse susceptibility was fit to the Curie-Weiss equation,  $C/(T - \Theta_{CW})$ . A Curie-Weiss temperature of  $-36$  K and an effective moment  $\mu_{eff}$  of  $4.38 \mu_B$  was determined for the data collected under a 10 kOe field. The effective moment lies between the spin-only value of  $3.87 \mu_B$  and the value of  $5.2 \mu_B$  expected for octahedrally coordinated  $\text{Co}^{2+}$  ( $d^7$ ,  $t_{2g}^5 e_g^2$ ,  $\mathbf{S}=3/2$ ,  $\mathbf{L}=3$ ) with a fully unquenched orbital contribution as obtained using the relationship  $\mu_{L+S} = \sqrt{4\mathbf{S}(\mathbf{S}+1) + \mathbf{L}(\mathbf{L}+1)}$ .<sup>24</sup> The existence of an orbital contribution is common from high-spin  $d^7$  systems in an octahedral  $d^7$  crystal field due to the orbital degeneracy in the  $t_{2g}$  levels. The small reduction of the orbital contribution likely arises from the irregular octahedral environment of the magnetic sites reducing some hybridization with the surrounding oxygen anions.

Fig. 2 shows the temperature dependence of the magnetic susceptibility of  $\text{CoSeO}_4$  under a variety of magnetic field strengths. The spins begin to order below 30 K which is very near the expected Curie-Weiss temperature indicating that there is very little frustration from competing exchange interactions. When measured in a 100 Oe field, a sudden jump in the susceptibility

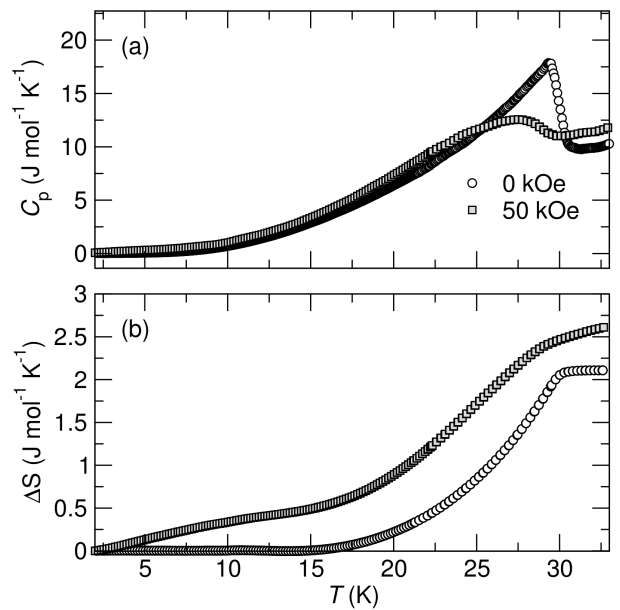


FIG. 4: (a) Temperature dependence of the specific heat of  $\text{CoSeO}_4$  measured on a powdered sample in  $H = 0$  kOe and 50 kOe field. (b) Entropy released due to the magnetic ordering, obtained by integration of the magnetic heat capacity.

occurs at 30 K which can be attributed to some weak ferromagnetism which results from a canted antiferromagnetic arrangement of the spins. Measuring the sample in larger fields minimizes the contribution from the weak-ferromagnetic component and gives rise to the cusp-like behavior expected from a well-compensated antiferromagnet. This cusp is found to broaden with increasing field strength indicating that the magnetic order may be driven to a different ground state in the presence of sufficiently large external fields. To further examine the nature of the field-dependence of the magnetic order, isothermal magnetization loops were collected at a variety of temperatures (Fig. 3). An upturn from the linear field-dependence expected for a well-behaved antiferromagnet is found beginning in a field of approximately 20 kOe at 28 K. The upturn shows a strong temperature dependence, with the field required to induce it increasing to 45 kOe by 18 K and subsequently out of the 50 kOe range of the magnetometer used here by 10 K. Such a field-induced magnetic transition may be attributed to overcoming of the magnetocrystalline anisotropy of the octahedral  $\text{Co}^{2+}$  cations which would manifest as a spin-flop transition where the spins realign from one preferred axis to another.

Fig. 4 (a) shows the specific heat of  $\text{CoSeO}_4$  measured in zero field, and under an external magnetic field of 50 kOe. The specific heat shows a sharp anomaly at the magnetic ordering temperature of 30 K in the absence of an external magnetic field. Application of a 50 kOe field results in a smearing out of the transition in a manner similar to the behavior observed in the susceptibility data shown in Fig. 2. The lattice contribu-

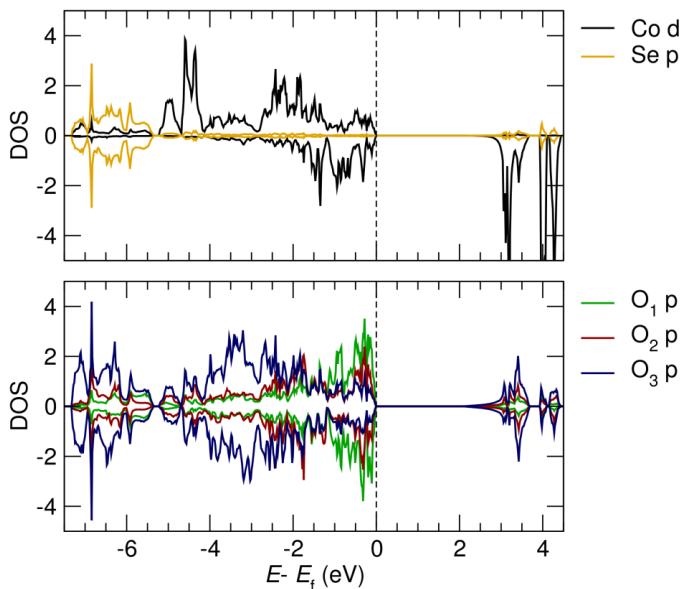


FIG. 5: (Color Online) Densities of state of  $\text{CoSeO}_4$  from a collinear spin structure calculation. The magnetic structure used in the calculation was that of antiferromagnetic chains aligned antiparallel to neighboring chains.

tion to the specific heat was approximated by fitting the data above the magnetic transition to a polynomial expansion ( $\beta T^3 + \gamma T^5 + \delta T^7$ ). Subtracting the lattice contribution and integrating  $C_p/T$  yields a change in entropy due to magnetic ordering of  $2.1 \text{ J mol}^{-1} \text{ K}^{-1}$  and  $2.5 \text{ J mol}^{-1} \text{ K}^{-1}$  in zero field and a 50 kOe field respectively. This value is significantly smaller than the value of  $11.5 \text{ J mol}^{-1} \text{ K}^{-1}$  predicted by the Boltzmann equation ( $\Delta S = R \ln(2\mathbf{S} + 1)$ ,  $\mathbf{S} = 3/2$ ). This considerable diminution of the spin entropy from what is expected may indicate that the reduced dimensionality of the system prevents complete ordering of the spins, or that possibly the order within chains is not well correlated with that in neighboring chains.

To better understand the electronic structure and chemical bonding in the title compound, density functional theory calculations were performed using the LDA+ $U$  formalism. Fig. 5 illustrates the density of states (DOS) calculated for the experimental room temperature structure of  $\text{CoSeO}_4$ . The DOS show a significant degree of overlap between the Se- $p$  and O- $p$  states and between Co- $d$  and O- $p$  states below the Fermi energy. However, there is a gap of approximately 250 meV between the Co and Se states. It can be seen that a majority of the Se and O overlap is related to bonding between Se and O<sub>3</sub>. The O<sub>3</sub> position forms two bonds within the Se tetrahedron which are 1.56 Å; short in comparison with the Se–O<sub>1</sub> and Se–O<sub>2</sub> bond lengths which are 1.74 Å and 1.78 Å respectively. Such bonding is consistent with the idea that the  $\text{SeO}_4$  tetrahedra contains two double and two single bonds with surrounding oxygens to satisfy its octet. It is interesting to note that the Se–O<sub>3</sub> bonds correspond

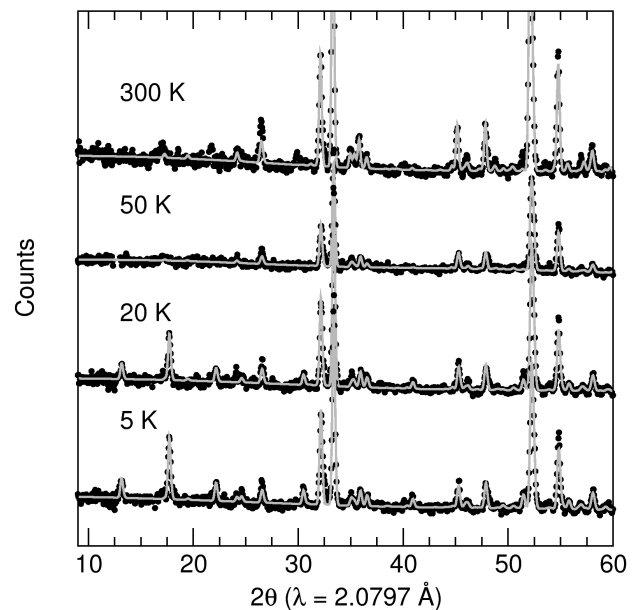


FIG. 6: Low angle region of the powder neutron-diffraction patterns of  $\text{CoSeO}_4$  (BT1,NIST) obtained at different temperatures.

to the shared oxygens at the corners of the  $\text{CoO}_6$  octahedra within a single chain. This arrangement of double bonds can be expected to significantly influence magnetic superexchange between the  $\text{CoO}_6$  chains.

The DOS calculated using the LDA formalism results in metallic densities of state, but by accounting for correlations within LDA+ $U$ , with  $U = 5 \text{ eV}$  and  $J = 1 \text{ eV}$ , a gap of approximately 3 eV opens between the occupied and unoccupied minority spins. We also note that the band gap which is approximately 2 eV corresponds to the gap between the highest filled states and unoccupied O- $p$  orbitals. The distorted octahedral environment of the  $\text{Co}^{2+}$  breaks the degeneracy of the unoccupied  $e_g$  orbitals corresponding to  $d_{z^2}$  and  $d_{x^2-y^2}$  with unoccupied  $d_{xz}$  above the Fermi energy.

The antiferromagnetic state is stabilized by more than 0.5 eV compared to a ferromagnetic alignment of spins. The calculated spin magnetic moment on each Co is  $2.72 \mu_B$  which is slightly reduced from the full value of  $3 \mu_B$  expected for a  $d^7$  cation in an octahedral coordination environment. Such a reduction may be associated with the covalent bonding to the surrounding oxygens or may be related to the fact that the calculation is restricted to a collinear spin configuration which is not the true ground state observed *via* neutron diffraction.

The thermal evolution of the neutron-diffraction patterns collected from 300 K to 5 K are shown in Fig. 6 with Table I showing a summary of refined parameters. Three magnetic reflections appear below 10 K at  $12^\circ$ ,  $18^\circ$ , and  $23^\circ$ , all of which are consistent with a propagation vector  $\mathbf{k} = 0$ . It was only possible to simultaneously fit all three magnetic peaks by using the basis vectors of the irreducible representation  $\Gamma_1$ . The resulting magnetic struc-

TABLE I: Summary of the results of Rietveld structure refinement of variable temperature neutron diffraction data obtained in zero magnetic field.

	300 K	20 K	5 K
$a$ (Å)	9.0421(3)	9.0355(4)	9.0344(4)
$b$ (Å)	6.7669(3)	6.7397(3)	6.7398(3)
$c$ (Å)	4.8860(2)	4.8759(2)	4.8757(2)
$M$ ( $\mu_B$ )	–	3.14(8)	3.50(8)
$V$ (Å <sup>3</sup> )	298.964(2)	296.927(2)	296.886(2)
$R_{\text{nuc.}}$ (%)	8.3	8.8	8.4
$R_{\text{mag.}}$ (%)	–	15.7	14.1

ture is illustrated in Fig. 8. The spins on each Co align antiferromagnetically down the length of the chain and with respect to the neighboring chains. The moment of each spin has components along all three axes of the unit cell as listed in Table II with a total magnetic moment of  $3.59 \mu_B$  at 5 K. The magnetic structure in the absence of a magnetic field shown in Fig. 8 agrees well with the previously reported structure of Fuess.<sup>14</sup> We note that while Fuess reported the structure in  $Pbnm$  we have chosen the standard setting of  $Pnma$ . The resulting spin configuration (compared to that reported by Fuess) has spins oriented largely in the  $ac$  plane with the moments tilting  $60^\circ$  ( $60^\circ$ ) off the  $a$ -axis,  $70^\circ$  ( $69^\circ$ ) off the  $b$ -axis, and  $44^\circ$  ( $41^\circ$ ) off the  $c$ -axis again at 5 K. The moment within individual chains do not cancel completely with a resulting uncompensated moment along the  $a$ -axis which is canceled by the neighboring chains. This uncompensated moment within the individual chains may be a source of the weak ferromagnetism observed in small external

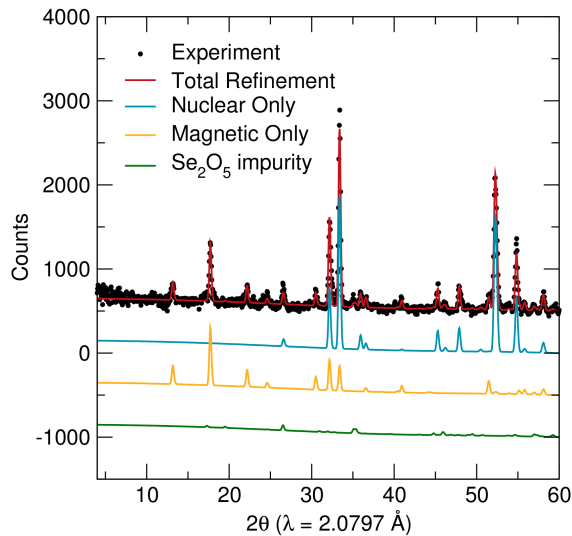


FIG. 7: (Color Online) Low angle region of the powder neutron-diffraction pattern of  $\text{CoSeO}_4$  obtained at 5 K and broken down in to the contribution from the nuclear, magnetic, and a small non-magnetic impurity phase of  $\text{Se}_2\text{O}_5$ .

magnetic fields.

The effect of applying a magnetic field of 70 kOe is to first reduce the total magnetic moment to  $2.60 \mu_B$  at 5 K. The field also causes the spins to reorient with respect to the unit cell. At 20 K the moments form angles of  $66^\circ$  off the  $a$ -axis,  $64^\circ$  off the  $b$ -axis, and  $37^\circ$  off the  $c$ -axis. From examination of the isothermal magnetization measurements in conjunction with the reorientated moments the field-induced magnetic transition appears to corresponds to a spin-flop transition on to the  $c$ -axis.

Fig. 9 (a) shows the inverse magnetic susceptibility normalized by the fits of the high temperature region (between 200 K and 300 K) to the Curie-Weiss formula. Normalizing in this manner emphasizes deviations from the Curie-Weiss equation in the form of short-range correlations between the spins which develop above the ordering temperature.<sup>25</sup> Fig. 9(b) shows the temperature dependence of the dielectric constant with a very clear change in slope in the dielectric constant at the magnetic ordering temperature.

To further characterize the coupling between the magnetism and dielectric properties, the dielectric constant was measured as a function of external magnetic field. A quadratic dependence of the dielectric constant with small fields was found and is shown in Fig. 10. Above

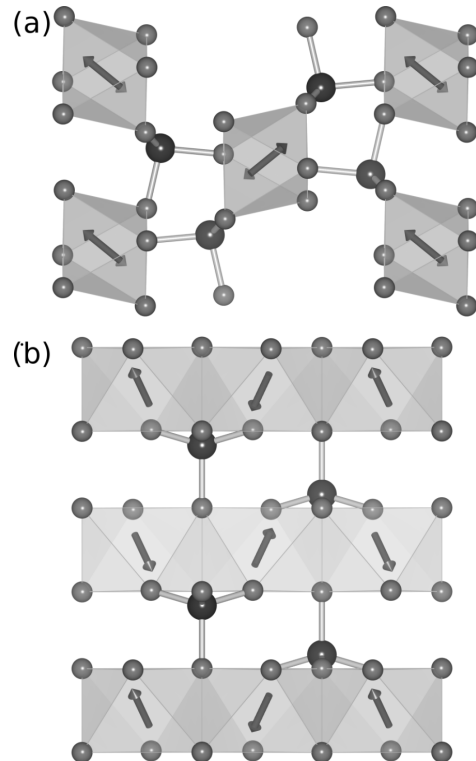


FIG. 8: Proposed magnetic structure of  $\text{CoSeO}_4$  as determined from Rietveld refinements of the neutron diffraction pattern obtained using a  $\lambda = 2.08 \text{ \AA}$  at 2 K. (a) View down the  $b$ -axis of the  $Pnma$  structure. (b) View down the  $c$ -axis. The small light grey atoms are oxygen while the larger and darker grey atoms are selenium

TABLE II: Components of the magnetic moment on each Co in the magnetic structure described by  $\Gamma_1$ . Note that Co at the origin occupies a  $4a$  Wyckoff site. The Co within the unit cell are: Co1 (0, 0, 0), Co2 ( $\frac{1}{2}$ , 0,  $\frac{1}{2}$ ), Co3 (0,  $\frac{1}{2}$ , 0), Co4 ( $\frac{1}{2}$ ,  $\frac{1}{2}$ ,  $\frac{1}{2}$ )

		0 kOe			70 kOe		
		$M_x$	$M_y$	$M_z$	$M_x$	$M_y$	$M_z$
20 K	Co1	1.51	1.05	2.51	0.86	0.93	1.68
	Co2	-1.51	-1.05	2.51	-0.86	-0.93	1.68
	Co3	-1.51	1.05	-2.51	-0.86	0.93	-1.68
	Co4	1.51	-1.05	-2.51	0.86	-0.93	-1.68
5 K	Co1	1.76	1.19	2.90	1.24	1.14	1.98
	Co2	-1.76	-1.19	2.90	-1.24	-1.14	1.98
	Co3	-1.76	1.19	-2.90	-1.24	1.14	-1.98
	Co4	1.76	-1.19	-2.90	1.24	-1.14	-1.98

the field-induced magnetic transition, the dielectric constant no longer exhibits a quadratic increase but rather changes abruptly to what appears to be a linear decrease. This could reflect the possibility that the low-field magnetic structure allows for a magnetodielectric response whereas the high-field magnetic structure does not. A similar temperature and field-dependent behavior has been reported by Nénert and coworkers<sup>26</sup> for a hy-

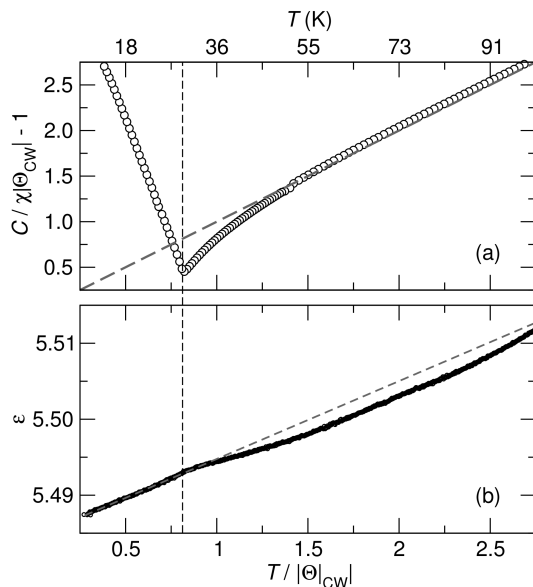


FIG. 9: (a) Inverse magnetic susceptibility normalized by the values extracted from fits to the Curie-Weiss formula in the high temperature region. Note that this manner of plotting emphasizes short-range correlations which cause deviations from ideal Curie-Weiss behavior which is illustrated as the dashed line. (b) Temperature dependence of the dielectric constant of CoSeO<sub>4</sub> measured on a pressed pellet of a polycrystalline sample at a frequency of 1 MHz. The dashed line is a guide-to-the-eye to emphasize the transition at the magnetic ordering temperature.

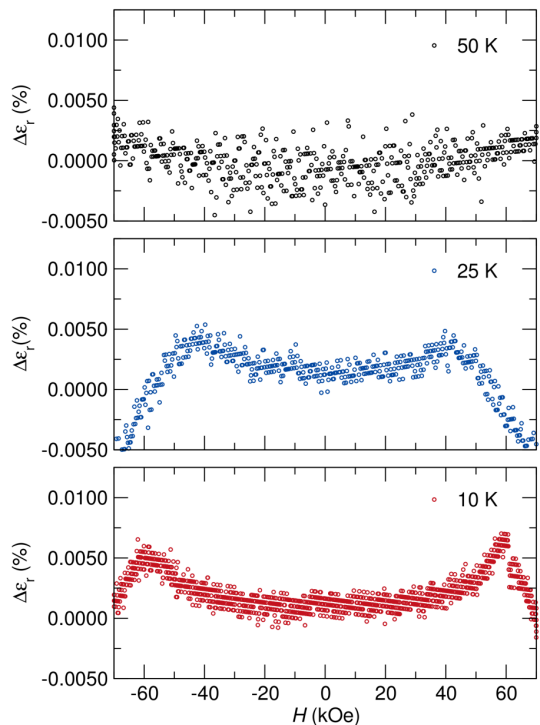


FIG. 10: Change in the dielectric constant measured at 1 MHz plotted as a function of the strength of the external magnetic field at different temperatures. Note the quadratic dependence until the field-induced magnetic transition

brid Cr(II) inorganic-organic material. They also find a quadratic change with external magnetic field above the magnetic ordering temperature as well as below and attribute the behavior to the always allowed  $P^2H^2$  order parameter. In that aspect, our results differ in that we see no response in the dielectric constant in the paramagnetic regime.

## Summary

We have discussed the preparation and detailed magnetic and dielectric characterization of a magnetic chain compound. Magnetization and specific heat measurements show a transition to a long-range canted antiferromagnetic state below 30 K and a temperature-dependent field-induced magnetic transition. Powder neutron diffraction shows the spins lay predominantly in the  $ac$ -plane with the moments tilting  $60^\circ$  off the  $a$ -axis,  $70^\circ$  off the  $b$ -axis, and  $44^\circ$  off the  $c$ -axis again at 5 K. Temperature and field dependent measurements of the dielectric constant show an anomaly at the magnetic ordering temperature, which, at fixed temperature, is quadratic in the external magnetic field. Temperature dependent measurements of the dielectric constant show an anomaly at the magnetic ordering temperature. We also find that the field-induced magnetic transition causes an abrupt change in the field dependence of the dielectric constant.

### Acknowledgements

The authors thank Daniel P. Shoemaker and Jonathan Suen for assistance in dielectric measurements. Support for this work came from the National Science Founda-

tion through a MRSEC award (DMR 0520415; support for BM and facilities), a Career Award (DMR 0449354) and the RISE program at the UCSB MRL (support of internships for LD and AG).

- 
- <sup>1</sup> G. Lawes, T. Kimura, C. M. Varma, M. A. Subramanian, N. Rogado, R. J. Cava, and A. P. Ramirez, *Prog. Solid State Chem.* **37**, 40 (2009).
- <sup>2</sup> N. Hur, S. Park, P. A. Sharma, S. Guha, and S.-W. Cheong, *Phys. Rev. Lett.* **93**, 107207 (2004).
- <sup>3</sup> Y. Yamasaki, S. Miyasaka, Y. Kaneko, J.-P. He, T. Arima, and Y. Tokura, *Phys. Rev. Lett.* **96**, 207204 (2006).
- <sup>4</sup> G. Lawes, B. Melot, K. Page, C. Ederer, M. A. Hayward, T. Proffen, and R. Seshadri, *Phys. Rev. B* **74**, 024413 (2006).
- <sup>5</sup> R. Tackett, G. Lawes, B. C. Melot, M. Grossman, E. S. Toberer, and R. Seshadri, *Phys. Rev. B* **76**, 024409 (2007).
- <sup>6</sup> G. Lawes, A. P. Ramirez, C. M. Varma, and M. A. Subramanian, *Phys. Rev. Lett.* **91**, 257208 (2003).
- <sup>7</sup> G. Lawes, A. B. Harris, T. Kimura, N. Rogado, R. J. Cava, A. Aharony, O. Entin-Wohlman, T. Yildirim, M. Kenzelmann, C. Broholm, et al., *Phys. Rev. Lett.* **95**, 087205 (2005).
- <sup>8</sup> K. Taniguchi, N. Abe, T. Takenobu, Y. Iwasa, and T. Arima, *Phys. Rev. Lett.* **97**, 097203 (2006).
- <sup>9</sup> T. Masuda, A. Zheludev, B. Roessli, A. Bush, M. Markina, and A. Vasiliev, *Phys. Rev. B* **72**, 014405 (2005).
- <sup>10</sup> S. Park, Y. J. Choi, C. L. Zhang, and S.-W. Cheong, *Phys. Rev. Lett.* **98**, 057601 (2007).
- <sup>11</sup> S.-W. Cheong and M. Mostovoy, *Nat. Mater.* **6**, 13 (2007).
- <sup>12</sup> T. Kimura, *Annu. Rev. Mater. Res.* **37**, 387 (2007).
- <sup>13</sup> H. Fuess and G. Will, *Z. Anorg. Allgemeine Chem.* **358**, 125 (1968).
- <sup>14</sup> H. Fuess, *Z. Angew. Phys.* **27**, 311 (1969).
- <sup>15</sup> V. Koleva and D. Stoilova, *Thermochim. Acta* **296**, 31 (1997).
- <sup>16</sup> H. Tanaka and M. Yamane, *J. Therm. Anal. Calorim.* **38**, 627 (1992).
- <sup>17</sup> G. Kresse and J. Furthmüller, *Phys. Rev. B* **54**, 11169 (1996).
- <sup>18</sup> G. Kresse and D. Joubert, *Phys. Rev. B* **59**, 1758 (1999).
- <sup>19</sup> P. E. Blöchl, O. Jepsen, and O. K. Andersen, *Phys. Rev. B* **49**, 16223 (1994).
- <sup>20</sup> D. M. Ceperley and B. J. Alder, *Phys. Rev. Lett.* **45**, 566 (1980).
- <sup>21</sup> H. J. Monkhorst and J. D. Pack, *Phys. Rev. B* **13**, 5188 (1976).
- <sup>22</sup> A. I. Liechtenstein, V. I. Anisimov, and J. Zaanen, *Phys. Rev. B* **52**, R5467 (1995).
- <sup>23</sup> C. Ederer and N. A. Spaldin, *Phys. Rev. B* **74**, 024102 (2006).
- <sup>24</sup> M. C. Day and J. Selbin, *Theoretical Inorganic Chemistry* (Reinhold Book Corporation, 1960), 2nd ed.
- <sup>25</sup> B. C. Melot, J. E. Drewes, R. Seshadri, E. M. Stoudenmire, and A. P. Ramirez, *J. Phys.: Condens. Matter* **21**, 216007 (2009).
- <sup>26</sup> G. Nénert, U. Adem, E. M. Bauer, C. Bellitto, G. Righini, and T. T. M. Palstra, *Phys. Rev. B* **78**, 054443 (2008).